Actinic inspection of extreme ultraviolet programed multilayer defects and cross-comparison measurements

Kenneth A. Goldberg[a)]
Lawrence Berkeley National Laboratory, Berkeley, California 94720

Anton Barty
Lawrence Livermore National Laboratory, Livermore, California 94550

Yanwei Liu
Lawrence Berkeley National Laboratory, Berkeley, California 94720

Patrick Kearney
SEMATECH, 255 Fuller Road, Suite 309, Albany, New York 12203

Yoshihiro Tezuka and Tsuneo Terasawa
MIRAI, Association of Super-Advanced Electronics Technologies, 16-1 Onogawa, Tsukuba, Ibaraki 305-8569, Japan

John S. Taylor
Lawrence Livermore National Laboratory, Livermore, California 94550

Hak-Seung Han and Obert R. Wood II
SEMATECH, 255 Fuller Road, Suite 309, Albany, New York 12203

(Received 23 June 2006; accepted 2 October 2006; published 30 November 2006)

The production of defect-free mask blanks remains a key challenge for extreme ultraviolet (EUV) lithography. Integral to this effort is the development and characterization of mask inspection tools that are sensitive enough to detect critical defects with high confidence. Using a single programed-defect mask with a range of buried bump-type defects, the authors report a comparison of measurements made in four different mask inspection tools: one commercial tool using 488 nm wavelength illumination, one prototype tool that uses 266 nm illumination, and two noncommercial EUV "actinic" inspection tools. The EUV tools include a dark field imaging microscope and a scanning microscope. Their measurements show improving sensitivity with the shorter wavelength non-EUV tool, down to 33 nm spherical-equivalent-volume diameter, for defects of this type. Measurements conditions were unique to each tool, with the EUV tools operating at a much slower inspection rate. Several defects observed with EUV inspection were below the detection threshold of the non-EUV tools. © *2006 American Vacuum Society.* [DOI: 10.1116/1.2375085]

I. INTRODUCTION

Operating near 13 nm wavelength, EUV projection lithography is reliant on nearly perfect reflective surfaces. Multilayer coatings applied across atomically smooth substrates give extreme ultraviolet (EUV) mirrors reflectivities as high as approximately 70%. The imaging lenses used in EUV lithography are arguably the highest quality optical imaging systems ever produced; they are typically comprised of two to six aspheric elements with surface figure and finish tolerances in the subnanometer range. Equally important are the patterned reticles fabricated with absorbing and/or phase-shifting features on thick mirror substrates.

Any disruption in the electric field reflected from the reticle has the potential to print on the wafer and cause device failure. Therefore the inspection of EUV reticles before and after patterning is critical to the success of EUV lithography. Given the increasing cost of a production mask set, accurate and reliable inspection potentially offers significant economic advantages in terms of mask cost. Speed and accuracy of inspection with sensitivity to the smallest printable defects is of primary concern, with mask blank inspection before patterning offering great potential to save mask makers from wasting time and effort on an imperfect substrate.

Separate from large-scale variations in the coating thickness, which cause a shift in the spectral response of the multilayer, small-scale defects are a particular concern. Many types of critical defects have been identified, including both *absorptive defects*[1,2] and *phase defects*.[3,4] EUV light is particularly susceptible to the presence of light-absorbing particles or thin layers of material on mirror surfaces; such defects can introduce phase shifts and significant local attenuation. Separately, *substrate defects*, bumps or pits, which are buried beneath the multilayer, can create local changes in the top surface profile. The reflectivity changes depend strongly on the multilayer deposition conditions,[5,6] but often these substrate defects will primarily affect the phase of the reflected light through path length differences or multilayer thickness effects, leaving the amplitude relatively constant.[4] For any defect type, reflection from the reticle typically enhances the deleterious effects by doubling the interaction path length or path length difference.

[a)]Electronic mail: kagoldberg@lbl.gov

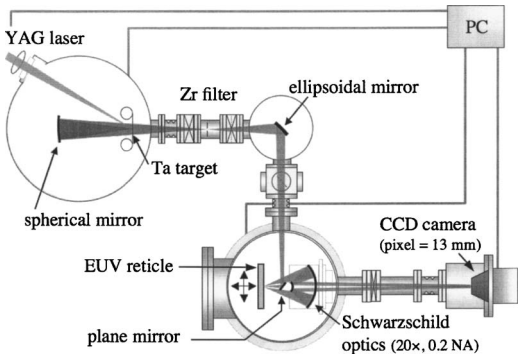

FIG. 1. Schematic of the MIRAI EUV mask inspection system which uses an annular Schwarzschild lens to project an image of the illuminated mask area onto an EUV CCD with 20× magnification.

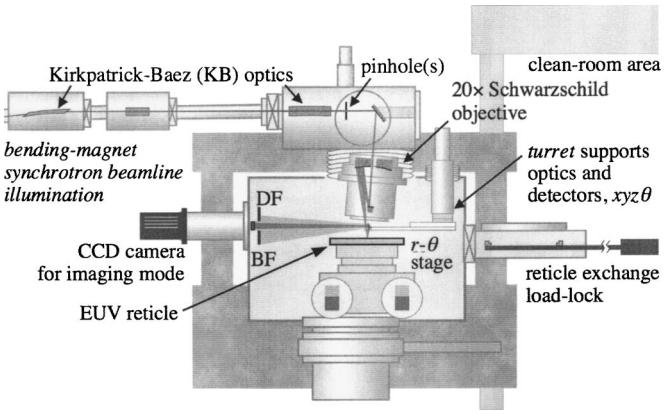

FIG. 2. Schematic of the dual-mode Berkeley EUV mask inspection system. In imaging mode it records high magnification mask images projected by a Fresnel zone plate onto an EUV CCD camera. In scanning mode a 1–5 μm beam traces a path across the mask surface while separate detectors record the bright field reflectivity and dark field scattered light.

Owing to the resonant-reflective properties of the multilayer coating, the nature and observability of reticle defects are highly wavelength dependent.[7,8] In particular, what constitutes a π-phase defect for EUV light may make insignificant changes at other wavelengths. Since most commercial mask blank inspection tools do not use EUV light, understanding the efficacy of these tools requires cross-comparison testing against EUV measurements and/or lithographic printing results, although currently, the utility of printing results for such a comparison can be limited by the resolution of experimental modern photoresist materials.[9] The comparison presented here represents the current state of the art, made with the best available data for a single programed-defect mask. Results for other programed-defect types and for native defects occurring with different multilayer deposition methods will be the subjects of future research.

II. EXPERIMENT DESCRIPTION

A single programed-defect mask was measured in four different mask inspection tools; the results are compared in this article. The mask was developed by Hoya and supplied by MIRAI (Serial No. MIRAI DEF03B), and some inspection results from this mask have been reported previously.[10,11] In addition to fiducial marks, it contains a 150×500 μm wide array of buried substrate defects created from 7-nm-thick CrN pads patterned below the multilayer coating. Defects of different sizes are arranged in nine columns with 49 similar defects per column. When measured with atomic force microscopy (AFM) after multilayer coating, the top surface shows two types of profiles: truncated (flat topped) pyramids (*TP type*) and Gaussian bumps (*G type*). The surface profiles range from 420 nm wide $\times$ 7 nm high, TP type, to as small as 70 nm wide $\times$ 3.5 nm high, G type for the smallest defects. A ninth column suffered from resist collapse leading to irregular sizes, and an intended tenth column did not print. In addition there is a rectangular border constructed of large defects surrounding the programed-defect array.

A. MIRAI dark field imaging tool

This mask was first measured with EUV light by Tezuka *et al.* using an EUV dark field imaging microscope developed by MIRAI.[10,11] In this system, shown in Fig. 1, a tantalum target is irradiated by a yttrium aluminum garnet laser producing EUV light, which is filtered by a Zr filter followed by an ellipsoidal mirror. Close to the mask, a small plane folding mirror directs the converging light toward the mask at normal incidence. Scattered, *dark field* light reflected from the reticle is collected by a 20× magnification Schwarzschild objective with an annular pupil subtending 0.1 to 0.2 numerical aperture, aligned at normal incidence to the mask. The objective projects the dark field image onto a low-noise scientific grade charge-coupled device (CCD) where an entire image field is recorded at once. Careful calibrations are performed to normalize the recorded signal.[11] The MIRAI tool was able to detect all of the programed defects with a high signal-to-noise ratio (SNR) and also note the presence of a few "native" defects that appeared after the measurements presented here.

B. Berkeley actinic inspection tool

The Berkeley actinic inspection system,[12] operated by Goldberg, Barty and Liu, illuminates the mask with EUV light yet records data in a much different manner than the MIRAI tool. As shown in Fig. 2, a bending magnet beamline at LBNL's Advanced Light Source provides monochromatic illumination to a pinhole; a 20× demagnification Schwarzschild objective reimages the illuminated pinhole onto the upward-facing reticle with a 6° angle of incidence. During measurement, the beam focus remains stationary while the mask is translated and rotated (r, θ) in a manner that allows a portion of the mask to be scanned. Using different pinhole diameters, the beam size on the reticle can be varied from 1 to 5 μm; these measurements were made with a 2.5 μm diameter beam.

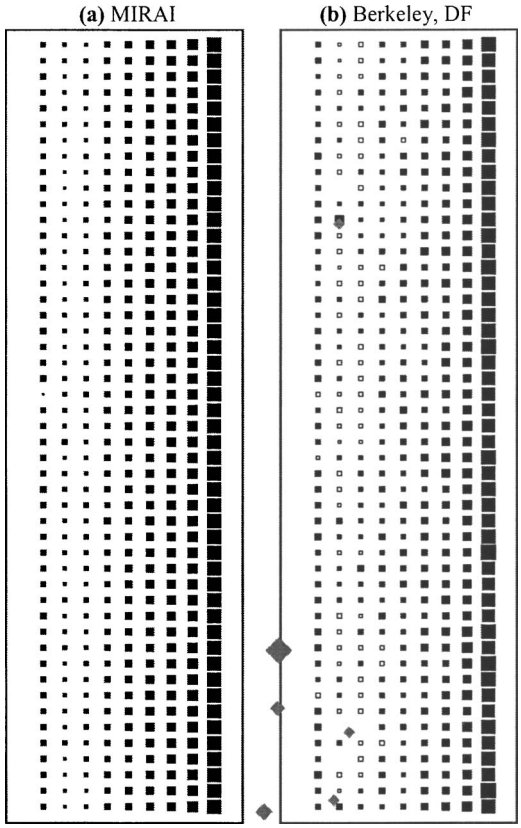

FIG. 3. EUV "actinic" inspections of the programed-defect region. (a) MIRAI tool data. (b) Berkeley tool dark field data. Square area corresponds to the measured SRN—figures are individually scaled for each tool. Open squares represent defects below 3.25σ detection threshold. Gray diamonds represent the relative size and location of surface contamination which occurred at some point after the MIRAI inspection shown here. Those dark regions were observed in the bright-field response measured with the Berkeley tool.

The Berkeley inspection system is flexible in its detector geometry and is capable of simultaneously recording bright field and dark field signals at up to 100 kHz. The inspection data presented here were recorded with a new detector design that records dark field light in an off-axis angular range of 0.6°–35° from the central ray in one direction and ±4.3° in the perpendicular direction, and with no intervening mirrors between the mask and the detector. In this way the dark field detection comes close to the specular beam; the detector was positioned to provide optimal SNR for the defects in this study.

C. Two Lasertec inspection tools

The test mask was also measured in two non-EUV inspection tools, both created by Lasertec Corp., and operated for these measurements by Kearney.

The Lasertec M1350, introduced in 2002, uses an argon-ion laser to generate light at the 488 nm illumination wavelength. The scanning confocal system uses a multiple image acquisition for gigabit inspection with confocal system configuration to achieve both high throughput and sensitivity. On transparent mask substrates, the M1350 can scan the entire 200 cm^2 quality area in 20 min; it has previously demonstrated polystyrene latex (PSL)-equivalent-size sensitivity below 60 nm.[7,8]

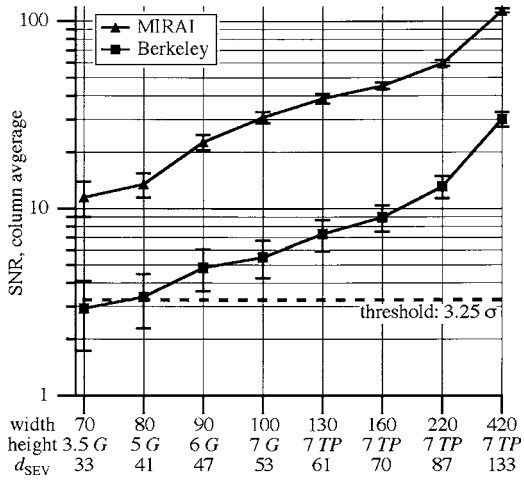

FIG. 4. Column averages of the measured SNR in the two EUV tools. For each column, the AFM-measured surface width and height of the defects are given in nanometers, along with the spherical-equivalent-volume diameter (d_{SEV}), also in nanometers. The defect surface shape is indicated with G for Gaussian and TP for truncated pyramid.

The mask was also measured in a new Lasertec inspection tool still under development at Lasertec. The Lasertec MB266 uses 266 nm wavelength ultraviolet light and operates in a similar manner to the M1350.

III. RESULTS

The comparison presented here represents the best available data from each tool as of June 2006. The methods and details of each individual measurement are quite different. The tools were designed to meet different performance metrics, and the data should be considered within the context of those differences. In particular, the Lasertec tools are designed for high throughput, large-area scanning. In contrast, the EUV tools are designed for research and were created to provide reference measurements for cross comparisons such as this. While each of the tools may be able to improve sensitivity by increasing the measurement time, this is especially true for the Lasertec tools, which scan mask areas from 40 to several thousand times faster than the EUV tools, depending on measurement conditions. We also note that the Lasertec MB266 had not yet been released at the time of measurement; as such, its sensitivity may continue to improve over time. For this reason, at Lasertec's request, only qualitative measurement results from this tool are presented.

For the two actinic tool measurements, the analysis presented here was performed on the raw inspection data. The defect strengths are compared with the background signal to determine the SNR of each measured defect in the array. The Lasertec tools report defect positions and sizes based on "pixels." The detection threshold for the Lasertec tools is set high (approximately 7σ) to avoid false positives within the measurement of the entire quality area of a mask under inspection.

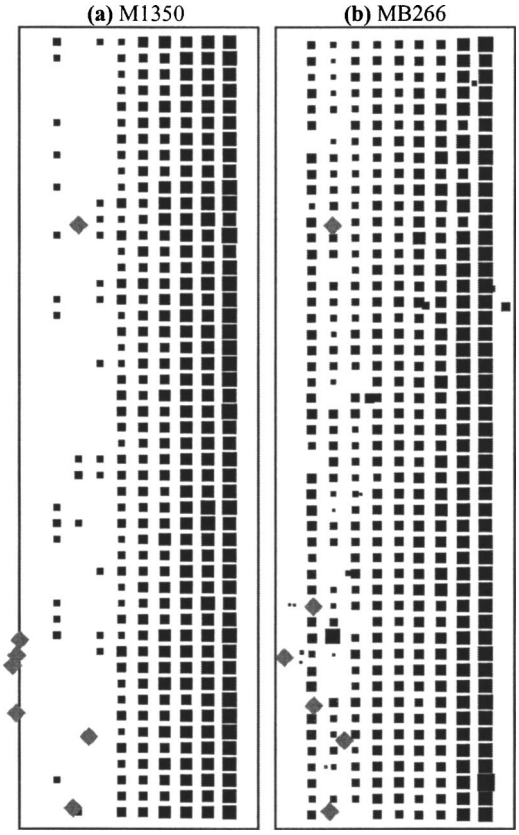

FIG. 5. Lasertec inspections of the programed-defect region: (a) M1350 (λ =488 nm) and (b) MB266 (λ=266 nm). The square areas correspond to the "pixel" size of the above-threshold defects. The positions of several native defects are shown as gray diamonds; their pixel size was reported as two to ten times higher than the largest programed defects.

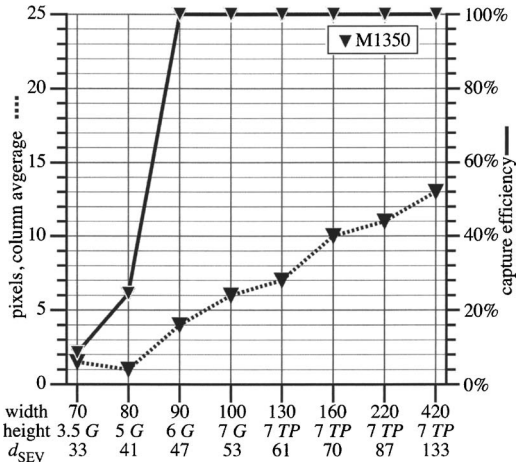

FIG. 6. Column averages of the measured pixel size (dashed line) for the defects above detection threshold as detected by the M1350. The capture efficiency (CE) is shown (solid line) for each defect size. Defect dimensions are given in nanometers.

A. Actinic inspection data

SNR calculations made from the inspection results of the two EUV tools are shown in Figs. 3 and 4. The MIRAI data are collected in the form of a single dark field image of the field. For the MIRAI tool, the SNR calculation is based on examining the integrated signal strength within an area of approximately 11 μm^2 centered at each known defect position. A careful normalization and background subtraction are performed using a local average over measured points between the defect positions. The noise level is calculated from an ensemble of 98 patches collected from defect-free regions of the image, treated in an identical manner as the defect regions.

The Berkeley data are acquired from a scanning measurement. Data were collected during a slow speed scan, with a 5 μm beam diameter on the mask and adjacent scan lines separated by 1 μm. For this measurement, the amplifier bandwidth limits independent measurements to approximately 0.1 μm separation in the scan direction. Following normalization to the background signal level, the raw data are used to reconstruct a two-dimensional *image* of the programed-defect region with 1 μm pixel grid. Once this image is calculated, the SNR calculation follows the same method applied to the MIRAI data, with local background subtraction, and the noise level calculated from 98 defect-free patches in adjacent areas of the same data set. A bright field scan of the region revealed the presence of a few native defects that appeared on the mask following the collection of the MIRAI data shown here. The calculation of the Berkeley tool's column-averaged SNR values excludes the programed defects covered by these native defects.

Relative to the measured noise level in small areas within defect-free areas, σ, a detection threshold value of 3.25σ was set for the EUV measurements, based on a 50% probability of a single false positive within the programed-defect region of interest.

B. Lasertec-tool inspection data

The Lasertec data, shown in Fig. 5, represent the *pixel* size of each defect found in the programed-defect region. Column averages for the pixel size of detected defects and the capture efficiency (CE) of the Lasertec M1350 are shown in Fig. 6. On this mask, the M1350 was able to detect 100% of defects down to 47 nm PSL-equivalent-volume diameter. The MB266 detected significantly more of the defects in the columns with the two smallest sizes.

IV. CONCLUSION

The interaction of reflected EUV light with defects on or below a mask surface is a complex process that is highly wavelength dependent. However, the necessity of EUV "actinic" inspection for the commercial production of defect-free EUV mask blanks remains an open question whose answer depends on sensitivity improvements in non-EUV inspection tools. The resonant-reflective properties of EUV multilayer coatings make cross comparison between EUV and non-EUV inspection tools critically important to the evaluation of new tools now under development and future tools as well. EUV inspection in both bright field and dark field modes provides quantitative feedback with high spatial

resolution in a manner that is beyond the capabilities of traditional reflectometers or printing tests. For evaluating surface defects, bump- and pit-type substrate defects, and novel defect-repair strategies, the cross comparison with EUV inspection will provide vital feedback and risk reduction.

We have inspected a bump-type buried substrate defect mask in four different states of the art inspection tools: two EUV research tools and two non-EUV tools produced by Lasertec. The EUV MIRAI dark field imaging tool was able to easily detect every defect on the mask with high SNR. The Berkeley tool detected most of the defects, down to the smallest sizes, with lower SNR than the MIRAI tool. The Berkeley tool also provides bright field reflectivity information, which clearly detects native surface defects. The Lasertec M1350, which operates at 488 nm wavelength, was able to detect 100% of the defects down to a 47 nm PSL-equivalent-volume diameter but had a lower capture efficiency below that level. The fourth tool was a prerelease Lasertec MB266, which operates at 266 nm wavelength and is significantly more sensitive to defects of this type than the M1350. The MB266 detected a majority of the defects at 33 and 41 nm, and, like the M1350, it detected 100% of the defects larger than those sizes. We note that the MB266 sensitivity may improve as the tool is optimized and that this data are based on a prerelease tool.

Additional comparisons involving defects of different sizes, shapes, and multilayer deposition methods will continue to provide quantitative data for tool evaluation and strategic decision making regarding the commercial need for actinic inspection of EUV masks. Of particular interest will be the future inspection of defect-repair strategies that may rely on the resonant-reflective multilayer properties to minimize disturbances of the EUV beam but may appear as defects in inspections performed at other wavelengths.

ACKNOWLEDGMENTS

The authors gratefully acknowledge funding support from SEMATECH under Contract No. LITH-343 and NEDO. The authors are also grateful to Hoya for providing the mask and Lasertec for their support of this work. CXRO scientific and technical staff members who have been instrumental in this work include Senajith Rekawa, C. Drew Kemp, Eric Gullikson, and others. Parts of this were performed under the auspices of the U.S. Department of Energy by the University of California, Lawrence Livermore National Laboratory under Contract No. W-7405-Eng-48 and Lawrence Berkeley National Laboratory under Contract No. DE-AC02-05CH11231.

[1]T. Liang, A. Stivers, R. Livengood, P.-Y. Yan, G. Zhang, and F.-C. Lo, J. Vac. Sci. Technol. B **18**, 3216 (2000).
[2]M. Yi, S. Jeong, S. Rekawa, and J. Bokor, J. Vac. Sci. Technol. B **18**, 2930 (2000).
[3]E. M. Gullikson, C. Cerjan, D. G. Stearns, P. B. Mirkarimi, and D. W. Sweeney, J. Vac. Sci. Technol. B **20**, 81 (2002).
[4]E. M. Gullikson, E. Tejnil, T. Liang, and A. R. Stivers, Proc. SPIE **5374**, 791 (2004).
[5]P. B. Mirkarimi and D. G. Stearns, Appl. Phys. Lett. **77**, 2243 (2000).
[6]D. G. Stearns, P. B. Mirkarimi, and E. Spiller, Thin Solid Films **446**, 37 (2004).
[7]E. M. Gullikson, E. Tejnil, K.-Y. Tsai, A. R. Stivers, and H. Kusunose, Proc. SPIE **5751**, 1223 (2005).
[8]K.-Y. Tsai, E. Gullikson, P. Kearney, and A. Stivers, Proc. SPIE **5992**, 1178 (2005).
[9]P. Naulleau *et al.*, Proc. SPIE **6151**, 61510Y (2006).
[10]Y. Tezuka, M. Ito, T. Terasawa, and T. Tomie, Proc. SPIE **5374**, 271 (2004).
[11]Y. Tezuka, M. Ito, T. Terasawa, and T. Tomie, Proc. SPIE **5567**, 791 (2004).
[12]Y. Liu, A. Barty, E. Gullikson, J. S. Taylor, J. A. Liddle, and O. Wood, Proc. SPIE **5751**, 660 (2005).